Journal of The Electrochemical Society, 2022 **169** 070523

Thermodynamic Analysis of the Hydrolysis of Borate-Based Lithium Salts by Density Functional Theory

Simone Di Muzio,[1] Oriele Palumbo,[1] Sergio Brutti,[1,2,3,z] and Annalisa Paolone[1]

[1]*Consiglio Nazionale delle Ricerche, Istituto dei Sistemi Complessi, 00185 Rome, Italy*
[2]*Sapienza University of Rome, Department of Chemistry, 00185 Rome, Italy*
[3]*GISEL-Centro di Riferimento Nazionale per i Sistemi di Accumulo Elettrochimico di Energia, 50121 Firenze, Italy*

Here we discuss the thermodynamics of the hydrolysis of three borate-based lithium salts commonly used in aprotic electrolytes for lithium-ion batteries: lithium tetrafluoroborate ($LiBF_4$), lithium difluoro(oxalate)borate (LiODBF) and lithium bis(oxalate)borate (LiBOB). We performed density functional theory calculations at the ωB97M-V/6–31++G** level to compute the thermodynamic stability of reagents, intermediate and products in solution phase. The variations of Gibbs free energy in heterogeneous reactions were evaluated by coupling DFT values with thermochemical cycles. $LiBF_4$ and LiODBF can be easily hydrolyzed by the direct reaction with water at room temperature: the salts degradation is driven by the precipitation of LiF(s) and by the release of HF. On the contrary, LiBOB is much more stable and only weakly reacts with water: it is therefore more resilient to hydrolyzation and therefore suitable for application in Li-ion battery electrolytes.

 [DOI: 10.1149/1945-7111/ac7ef2]

Manuscript submitted April 18, 2022; revised manuscript received June 22, 2022. Published July 20, 2022.

Supplementary material for this article is available online

Lithium-ion batteries (LIBs) are one of the most popular portable energy storage systems and are used in a plethora of devices and applications, despite their cost. The excellent performance, in terms of number of cycles, electrochemical stability and energy density overcomes any existing competitive technology.[1,2] A long lasting calendar life of LIBs is driven by the effective electrolytes, which are usually constituted by aprotic solvents and lithium salts, and characterized by low viscosity and large ionic conductivities, lithium transference number and electrochemical stability windows.[3] Indeed, the choice of a specific lithium salt is driven by its chemical-physical properties, i.e. chemical and thermal stability, large electrochemical stability windows, low toxicity and considerations concerning costs. The most popular salts used in LIBs contain large amounts of fluorine, like lithium hexafluorophosphate ($LiPF_6$) and lithium tetrafluoroborate ($LiBF_4$). Other common salts are lithium bis(oxalate)borate (LiBOB[4]), lithium difluoro(oxalate)borate (LiODBF[5]) and lithium sulfonyl-imide (LiFSI[6] and LiTFSI). $LiBF_4$is able to provide performances close to those of $LiPF_6$,[7] it is more stable at high temperature, showing improved cycling performances compared to $LiPF_6$,[8] as well as at low temperatures.[9] Overall, the performances of electrolytes based on $LiBF_4$are remarkable, thus making this salt a valuable alternative to $LiPF_6$.

Unfortunately, the presence of traces of undesired water can trigger the hydrolysis of lithium salts in aprotic solvents; as a consequence, the water content must be minimized or possibly completely suppressed. To this aim many strategies have been developed, like sequestration of water in batteries by functional separators[10,11]or ceramic fillers.[12,13] Salts hydrolysis is a key-step of the degradative reactivity of electrolytes, either chemical or electrochemical as it contributes to the formation of solid electrolyte interface (SEI)[14] over the electrode surfaces. The complete mechanism for the formation of these passivation films on the surface of the electrodes is really complex and it is typically studied coupling various experimental approaches, such as FT-IR, Raman and XPS spectroscopies,[15] X-ray diffraction.[16] Experiments can be further coupled to computational methods, as ab initio and DFT calculations,[17] classic and first principle molecular dynamic simulations[18,19] and multiscale approaches[20] to elucidate the SEI precipitation mechanism at the atomic scale. The formation of a proper SEI is very important as it allows a successful operation of batteries, whereas the uncontrollable accumulation of solids on the surface of electrodes reduces the amount of lithium ion in the electrolyte.[21] The kinetics of the hydrolysis of lithium salts has been discussed by many authors:[22,23] the thermodynamic landscape is complex, especially considering the contribution of precipitation of solid compounds, the formation of gaseous byproducts and/or unexpected soluble species.

Focusing on boron-containing salts the degradation of BF_3 has been investigated by experimental approaches,[24] to shed light on the hydrolysis of $LiBF_4$. LiBOB is the fluorine free analogue of $LiBF_4$ and, for this reason, it has been proposed and demonstrated in many LIBs formulations.[25] Furthermore, LiBOB is even indicated as a possible replacement of $LiPF_6$ thanks to the improved thermal stability[26] and environmental benignity. In analogy to LiBOB and $LiBF_4$, also LiODBF exhibits good electrochemical performances in LIBs, especially in high-concentrated solutions and at high temperatures.[27]

In this study we discuss the thermodynamic landscape of the hydrolysis pathways of $LiBF_4$, LiBOB and LiODBF (Fig. 1) by electronic structure calculations using the density functional theory (DFT). To this aim, we adopted a methodological approach already validated by us in a previous paper:[28] we exploited an implicit model of solvation (PCM) to mimic the thermodynamic stability of soluble species in aprotic solvents, while the effect of the precipitation of insoluble compounds was described by thermodynamic cycles.[28] Our final goal is to investigate how the hydrolysis of lithium salts contributes to the complex reaction pathways that lead to the formation of SEI in LIBs.

Methods

The electronic structure of neutral molecules, either radical with odd electrons or closed shell, ions and atoms were modeled by DFT. All species and their optimized structures were computed using the Spartan20[29] software. The Range Separated meta-GGA ωB97M-V[30] functional was adopted with a 6–31++G** basis set.[31] Singlet or doublet spin states were assumed for all closed shell and radical species, respectively: spin contamination has been checked in preliminary tests. The choice of ωB97M-V/6–31++G** is a good compromise between computational costs and accuracy (see below). Geometrical conformers were identified using the molecular mechanics algorithm inbuilt in Spartan20. Equilibrium geometries were computed by structural relaxations of the atomic positions and verified by vibrational frequencies calculations. Electronic energies

[z]E-mail: sergio.brutti@uniroma1.it

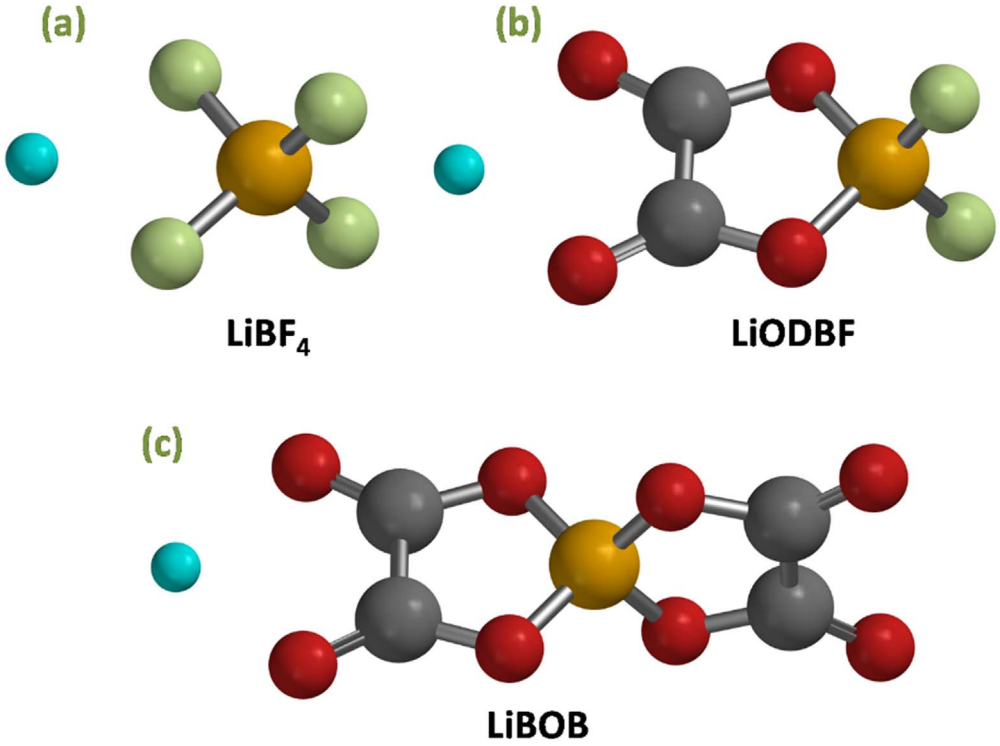

Figure 1. Optimized structures of lithium salts: (a) lithium tetrafluoroborate ($LiBF_4$), (b) lithium difluoro(oxalate)borate (LiODBF), (c) lithium bis(oxalate) borate (LiBOB). (Oxygen = red, Fluorine = green, Carbon = grey, Boron = orange, Lithium = cyan).

and vibrational contributions were evaluated assuming an implicit solvation model (Polarizable Continuum Model, PCM[32]), to simulate a polar environment ($\varepsilon = 37.22$). Free Gibbs energy was computed for each chemical species by evaluating the partition functions and considering the zero-point energies. Free Gibbs Energy, $\Delta_r G_T^0$, of reactions were calculated as stoichiometrically-weighed algebraic sums between the Gibbs Free Energy of products and reactants.

The computational accuracy of ωB97M-V/6–31++G** was evaluated comparing the thermodynamics of a set of reactions with similar calculations carried out by B3LYP[33] and the benchmarks MP2 and CCSD(T) methods, using the same basis set (see the Supporting Info). The relative errors in terms of Gibbs energy of reaction accuracy compared to MP2 calculations are 11.6% in the case of ωB97M-V/6–31++G** and 14.3% for B3LYP/6–31++G** and thus the ωB97M-V functional outperforms the popular B3LYP. Turning to the relative errors in terms of total energy of reaction at 0 K calculated by comparing the DFT total electron energies with the corresponding CCSD(T) data are 4.1% in the case of ωB97M-V/6–31++G** and 16.1% for B3LYP/6–31++G**. Again, the ωB97M-V functional outperforms the popular B3LYP. The stoichiometry of all reactions, energies and relative errors are summarized in Tables SI–SV in Supplementary Information (SI)(available online at stacks.iop.org/JES/169/070523/mmedia). Cartesian coordinates of the relaxed structures of all relevant reagents, intermediates and products are reported in the SI (Table SVI).

In order to evaluate the possible occurrence of heterogeneous reactions, we coupled DFT-based thermodynamics in solvents with the thermodynamic cycles shown in Fig. 2. In fact, a direct computation of the thermodynamics of heterogeneous reactions is not feasible using our computational approach but can be achieved by exploiting the thermochemical methodology already proposed by us,[28] consisting in a general approach to calculate the effect of the precipitation based on thermochemical cycles, as described in Fig. 2. In this framework, the precipitation thermodynamics of a generic compound $A_aB_bC_c$ is described combining the DFT data on molecules with assessed literature thermodynamic quantities obtained from standard thermodynamic database.[34] Here we extended the use of thermochemical cycles to the description of the precipitation of boric acid and oxalic acid. Assuming the notation in Fig. 2, the precipitation of the solvated $A_aB_bC_c$(sol) species is driven by the thermodynamics of reaction R. On the other hand, the Gibbs energy of reaction R is also given by the following set of thermochemical equations:

$$\Delta_r G_T^0(R) = \Delta_r G_T^0(R^a) + \Delta_r G_T^0(R^b) + \Delta_r G_T^0(R^c) \qquad [R]$$

Atomization of $A_aB_bC_c$ (solvated):

$$\Delta_r G_T^0(R^a) = a\Delta G_T^{tot,DFT}(A(g)) + b\Delta G_T^{tot,DFT}(B(g)) + c\Delta G_T^{tot,DFT}(C(g)) - (A_aB_bC_c(sol)) \qquad [Ra]$$

Formation of the monoatomic gas:

$$\Delta_r G_T^0(R^b) = a\Delta_f G_T^0(A(g)) + b\Delta_f G_T^0(B(g)) + c\Delta_f G_T^0(C(g)) \qquad [Rb]$$

Formation of $A_aB_bC_c$ (solid):

$$\Delta_r G_T^0(R^b) = \Delta_f G_T^0(A_aB_bC_c(s)) \qquad [Rc]$$

Where *s* stands for solid phase, *g* for gas phase and *sol* for solution phase.

Examples of thermochemical cycle to derive the precipitation thermodynamics of LiOH, LiF, H_3BO_3 and $H_2C_2O_4$ are shown in Figs. 2B–2E.

Results

$LiBF_4$ hydrolysis in simulated aprotic solvent.—The Potential Energy Surface (PES) calculated to mimic the hydrolysis of $LiBF_4$ is shown in Fig. 3. It is important to underline that all steps where solid phases are present have been computed by combining firsts principle computations in simulated solvents with thermodynamic cycles

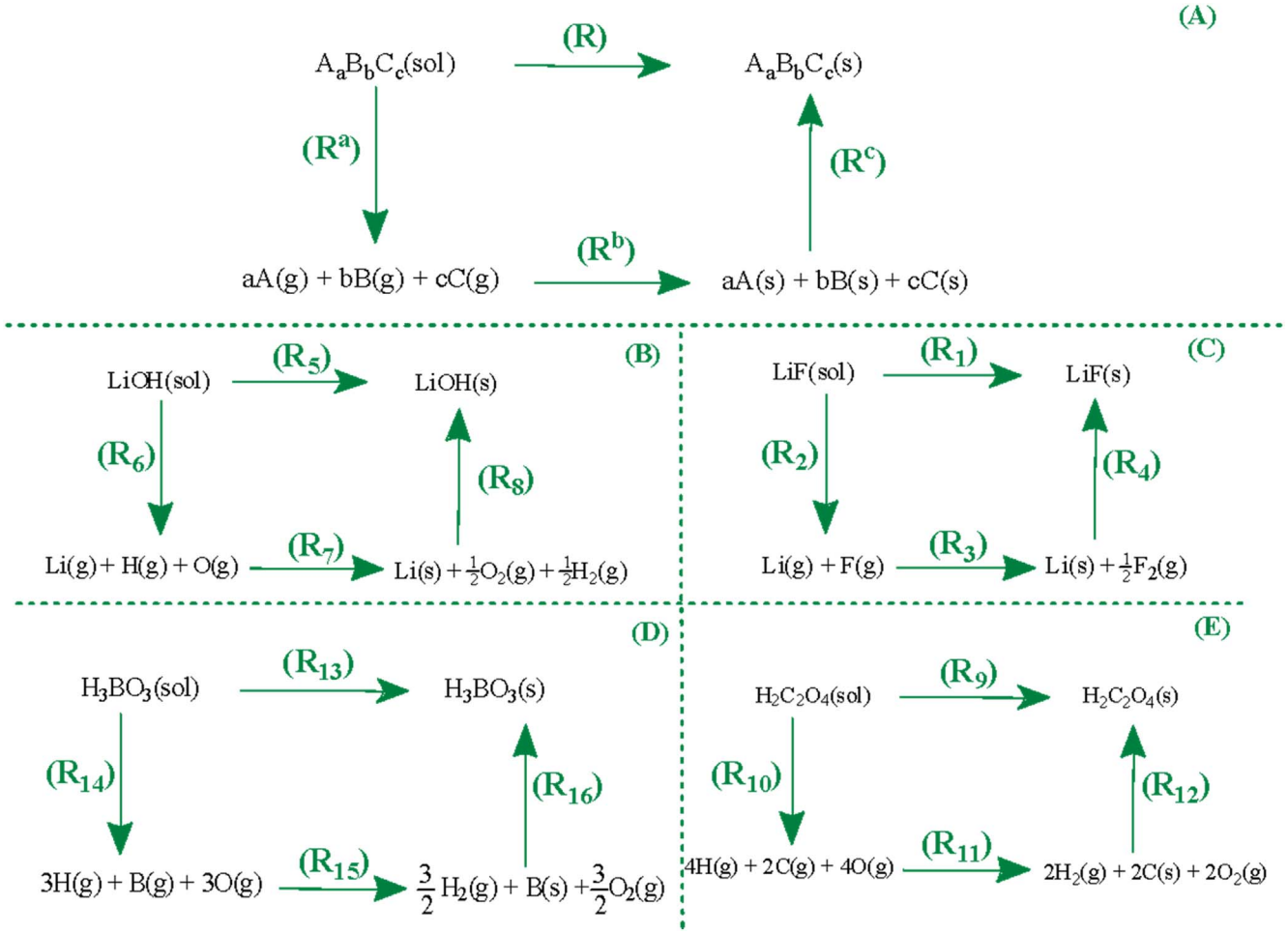

Figure 2. (A) General reaction cycle for the description of the thermodynamic of precipitation R of a generic molecule $A_aB_bC_c$.; Reaction cycle for the description of the thermodynamics of the precipitation of LiOH(s) (B), LiF(s) (C), H_3BO_3(s) (D) and $H_2C_2O_4$(s) (E).

whereas all reactions in the homogeneous simulated solvent are predicted uniquely from the computational modeling results.

In aprotic solvents Li^+ is strongly coordinated to the BF_4^- anion by a direct coulombic ionic interaction. This ionic couple can unlikely undergo to the ionic dissociation R1:

$$LiBF_4 \rightleftarrows Li^+ + BF_4^- \qquad [R1]$$

being the computed $\Delta_r G^o_{298K}$ R1 = 74 kJ mol^{-1}. Other simple reactions involving $LiBF_4$ are the Lewis acid/base equilibria R2:

$$LiBF_4 \rightleftarrows LiF(s) + BF_3 \qquad [R2a]$$

$$LiBF_4 \rightleftarrows LiF(sol) + BF_3 \qquad [R2b]$$

The dissociation of lithium tetrafluoroborate leads to the formation of trifluoroborane (BF_3) and lithium fluoride. The thermodynamic of R2 is strongly altered by the precipitation of LiF; in fact, the computed $\Delta_r G^o_{298K}$ R2a is −25 kJ mol^{-1}, whereas $\Delta_r G^o_{298K}$ R2b is strongly positive (120 kJ mol^{-1}). Turning to the direct reaction with water, lithium tetrafluoroborate can follow two competitive mechanisms:

$$LiBF_4 + H_2O \rightleftarrows \frac{1}{3}B_3O_3F_3 + 2HF + LiF(s) \qquad [R3a]$$

$$LiBF_4 + H_2O \rightleftarrows BOF + 2HF + LiF(s) \qquad [R3b]$$

Reaction R3a is exergonic, i.e. $\Delta_r G^o_{298K}$ R3a is −15 kJ mol^{-1}. In this reaction two factors push the equilibrium in favor of the products: the precipitation of LiF(s) and the formation of trifluoroborexine ($B_3O_3F_3$), as already described in previous works.[35–37] The trimerization of BFO to give $B_3O_3F_3$:

$$BFO \rightleftarrows \frac{1}{3}B_3O_3F_3 \qquad [R4]$$

is strongly exergonic, with $\Delta_r G^o_{298K}$ R4 = −170 kJ mol^{-1}. As a consequence, R3b unlikely occurs, because the computed $\Delta_r G^o_{298K}$ R3b equals 155 kJ mol^{-1}.

The hydrolysis mechanism of BF_3 is well known from a previous work.[38] BF_3 can easily react with water forming hydrofluoric acid and BF_2OH:

$$BF_3 + H_2O \rightleftarrows BF_2OH + HF \qquad [R5]$$

Reaction R5 is a nucleophilic addition, and it is weekly exergonic, with $\Delta_r G^o_{298K}$ R5 = −8 kJ mol^{-1}. Considering a similar mechanism described for $LiBF_4$, boron trifluoride can also follow a parallel reactive channel as described in R6:

$$BF_3 + H_2O \rightleftarrows \frac{1}{3}B_3O_3F_3 + 2HF \qquad [R6]$$

However, R6 reaction is slightly endergonic ($\Delta_r G^o_{298K}$ R6 = 10 k J mol^{-1}). Once formed, BF_2OH can further hydrolyze by another water addition:

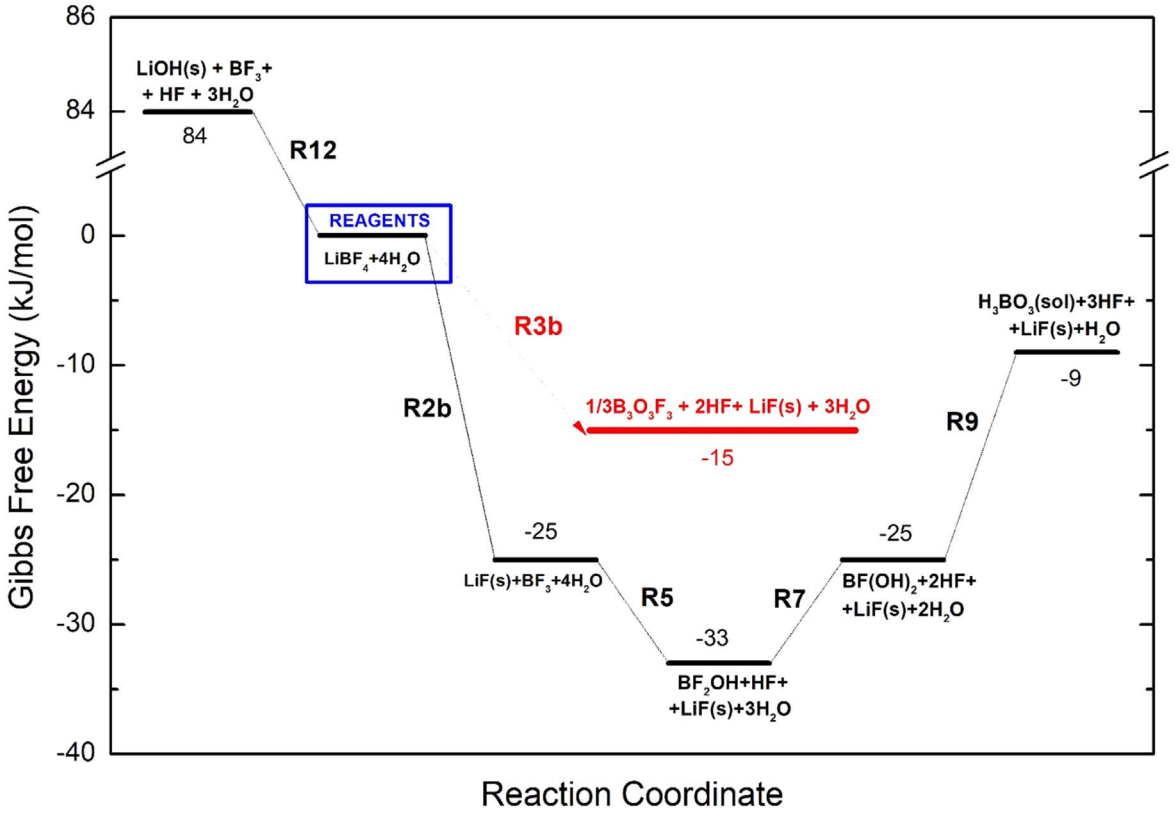

Figure 3. Potential Energy Surface (PES) for $LiBF_4$ hydrolysis. Steps implying the formation of LiF(s) and Li(OH) have been derived considering implicit thermodynamic cycles (see the methodology section). Numerical values close to the energy levels are the corresponding Gibbs energy differences compared to reagents.

$$BF_2OH + H_2O \rightleftarrows BF(OH)_2 + HF \quad [R7]$$

Reaction R7 is moderately endergonic, as $\Delta_r G^o_{298K}$ R7 = 8 kJ mol^{-1}. Also in this case, an additional competitive path leads to the formation of $B_3O_3F_3$:

$$BF_2OH + H_2O \rightleftarrows \frac{1}{3}B_3O_3F_3 + HF \quad [R8]$$

However, reaction R8 is thermodynamically unfavorable, because $\Delta_r G^o_{298K}$ R8 = 18 kJ mol^{-1}. Starting from $BF(OH)_2$ also a third water addition may occur leading to the formation of boric acid and the release of hydrofluoric acid:

$$BF(OH)_2 + H_2O \rightleftarrows H_3BO_3 + HF \quad [R9]$$

This reaction is endergonic, with a moderate change of the Gibbs Free energy $\Delta_r G^o_{298K}$ R9 = 16 kJ mol^{-1}.

All these reactions occur in solution without precipitation of by-products apart from LiF(s) in reaction R2a. In fact, the precipitation of boric acid R10 is endergonic, $\Delta_r G^o_{298K}$ R10 = 22 kJ mol^{-1}:

$$H_3BO_3(sol) \rightleftarrows H_3BO_3(s) \quad [R10]$$

$BF(OH)_2$ can also react with a molecule of water, forming a molecule of $B_3O_3F_3$, through the endergonic reaction R11:

$$BF(OH)_2 \rightleftarrows \frac{1}{3}B_3O_3F_3 + H_2O \quad [R11]$$

Being $\Delta_r G^o_{298K}$ R11 equal to 10 kJ mol^{-1}. Besides these mechanisms, $LiBF_4$ can react with water leading to the release of lithium hydroxide via an acid/base equilibrium, as described in R12:

$$LiBF_4 + H_2O \rightleftarrows BF_3 + LiOH(s) + HF \quad [R12]$$

However, the formation of LiOH can be excluded since the thermodynamics of R12 is strongly endergonic, both in solution and in heterogeneous phase, given that $\Delta_r G^o_{298K}$ R12 = 84 kJ mol^{-1}.

LiODBF hydrolysis in simulated aprotic solvent.—The thermodynamic landscape computed for the hydrolysis of LiODBF is shown in the Fig. 4, where the stoichiometry of two competitive paths is also reported.

$Li^+$is strongly coordinated to $ODBF^-$via a delocalized Coulombic interaction, as the partial negative charges are sitting on the carbonylic oxygens of the counter anion. In this respect the binding between anion and cation is strong being the ionic dissociation of LiODBF R13 endergonic:

$$LiODBF \rightleftarrows Li^+ + ODBF^- \quad [R13]$$

In fac the $\Delta_r G^o_{298K}$ R13 = 83 kJ mol^{-1} a value that suggest a close interaction between anion and cation in the solvent and a very limited ionization. The second reaction is a Lewis acid/base equilibrium R14 similar to R3 for $LiBF_4$:

$$LiODBF \rightleftarrows LiF(s) + ODBF \quad [R14]$$

This reaction is slightly endergonic, with $\Delta_r G^o_{298K}$ R14 equal to 19 kJ mol^{-1}.

Starting from the electron poor ODBF molecule the hydrolysis degradation onsets from the nucleophilic attack to form the intermediate product M_1 (see Fig. 2a) thought reaction R15:

$$ODBF + H_2O \rightleftarrows M_1 + HF \quad [R15]$$

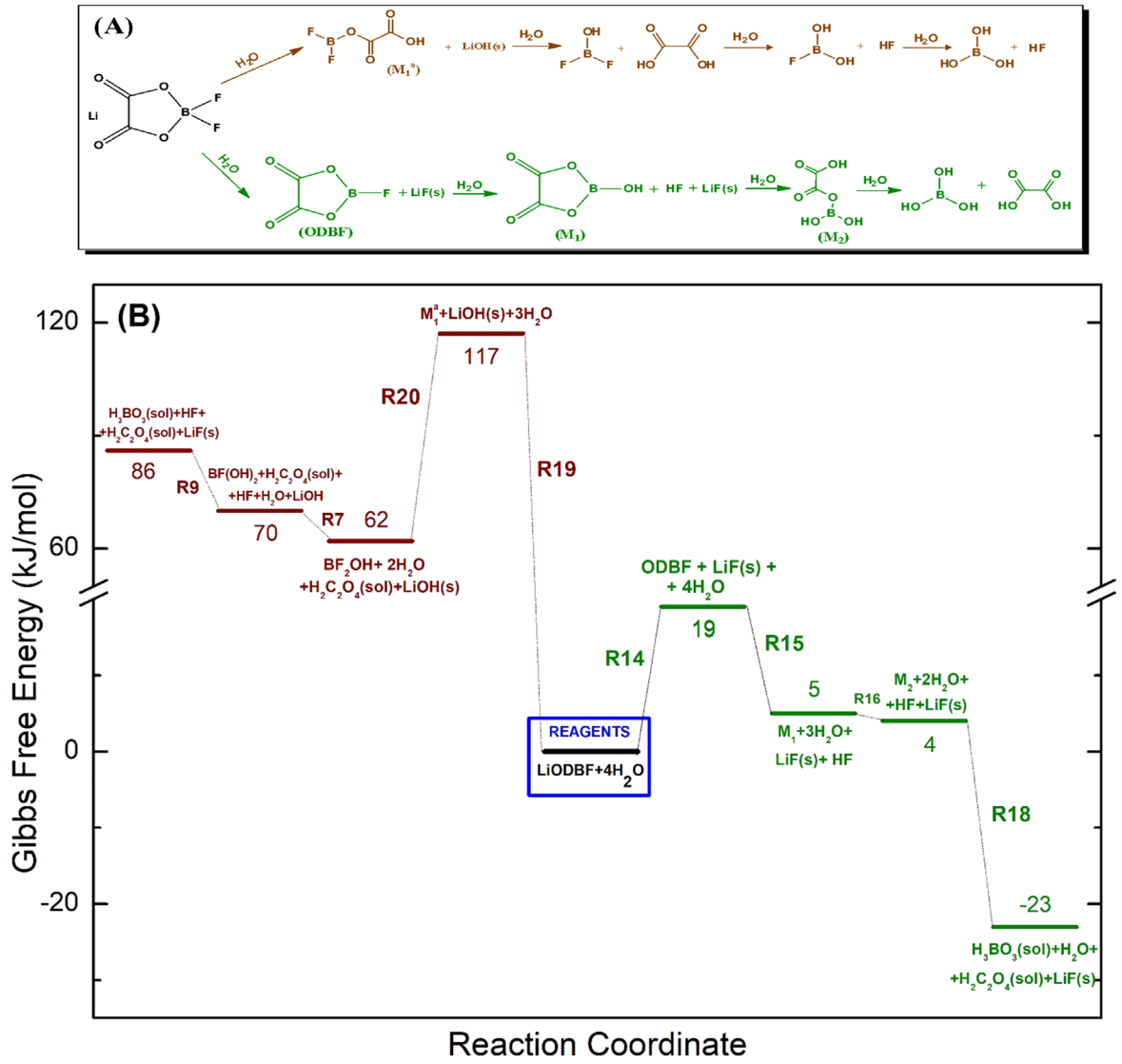

Figure 4. (A) Reaction pathways for the hydrolysis of LiODBF; (B) Potential Energy Surface (PES) for LiODBF hydrolysis. Steps implying the formation of LiF(s) and Li(OH) have been derived considering implicit thermodynamic cycles (see the methodology section). Numerical values close to the energy levels are the corresponding Gibbs energy differences compared to reagents.

Reaction R15 is exergonic being $\Delta_r G^o_{298K}$ R15 $= -14$ kJ mol^{-1}. The addition of another molecule of water leads to the formation of M_2 (see Fig. 2a):

$$M_1 + H_2O \rightleftarrows M_2 \qquad \text{[R16]}$$

The ring-opening mechanism is weakly exergonic, with a Gibbs Free energy variation $\Delta_r G^o_{298K}$ R16 $= -1$ kJ mol^{-1}. The heterolytic cleavage of the boron-oxygen bond in M_2 can easily release boric acid and oxalic acid following reaction R17:

$$M_2 + H_2O \rightleftarrows H_3BO_3(sol) + H_2C_2O_4(sol) \qquad \text{[R17]}$$

Reaction R17 is exergonic ($\Delta_r G^o_{298K}$ R17 $= -27$ kJ mol^{-1}). Once formed, $H_2C_2O_4$ does not precipitate, because the corresponding thermodynamics is endergonic, i.e. $\Delta_r G^o_{298K}$ R18 $= 11$ kJ mol^{-1}:

$$H_2C_2O_4(sol) \rightleftarrows H_2C_2O_4(s) \qquad \text{[R18]}$$

Keeping in mind the reaction energies of R18 and R10, we can exclude massive precipitations of boric acid and oxalic acid through this hydrolysis path.

An alternative pathway of the hydrolysis of LiODBF has been also considered starting from a direct nucleophilic addition of water to give LiOH and M_1^a (see Fig. 2a):

$$LiODBF + H_2O \rightleftarrows M_1^a + LiOH\,(s) \qquad \text{[R19]}$$

Reaction R19 is strongly endergonic, being $\Delta_r G^o_{298K}$ R19 $=$ 117 kJ mol^{-1}. M_1^a can react again with water: in this case the formation of BF_2OH and the release of oxalic acid is favored, given that $\Delta_r G^o_{298K}$ R20 $= -55$ kJ mol^{-1}:

$$M_1^a + H_2O \rightleftarrows BF_2OH + H_2C_2O_4 \qquad \text{[R20]}$$

Once formed BF_2OH may follow the degradation path described in the previous section (R7 and
R9). Overall, despite the large exergonicity of R20, the remarkable positive energy difference between reagents and products of reaction R19 likely hinders this chemical hydrolyzation path.

LiBOB hydrolysis in simulated aprotic solvent.—The PES of the hydrolysis of LiBOB is shown in Fig. 5.

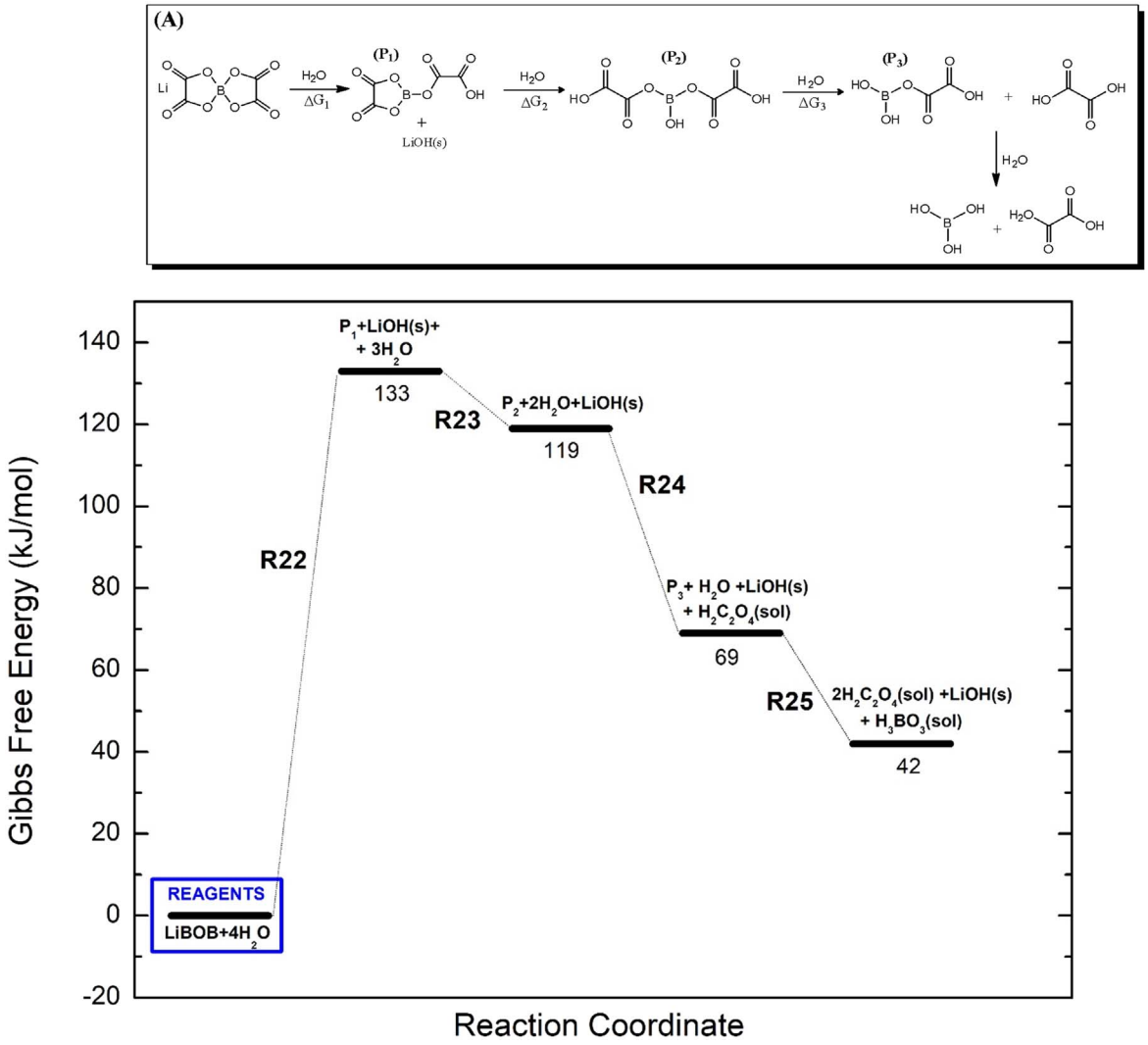

Figure 5. (A) Reaction pathways for the hydrolysis of LiBOB; (B) Potential Energy Surface (PES) for LiBOB hydrolysis. Steps implying the formation of Li (OH) have been derived considering implicit thermodynamic cycles (see the methodology section). Numerical values close to the energy levels are the corresponding Gibbs energy differences compared to reagents.

In aprotic solvents Li^+ is strongly coordinated to BOB^-. This ionic couple can dissociate following reaction R21:

$$LiBOB \rightleftarrows Li^+ + BOB^- \qquad [R21]$$

This reaction is endergonic with a $\Delta_r G^o_{298K}$ R21 = 77 kJ mol^{-1}. LiBOB can undergo a nucleophilic water addition R22, forming the intermediate product P_1 (see Fig. 5a):

$$LiBOB + H_2O \rightleftarrows P_1 + LiOH(s) \qquad [R22]$$

Reaction R22 is strongly endergonic ($\Delta_r G^o_{298K}$ R22 = 133 kJ mol^{-1}) and, therefore, this reaction unlikely occurs. Once formed P_1 can undergo a nucleophilic attack by a second water molecule, forming the intermediate P_2 (see Fig. 5a):

$$P_1 + H_2O \rightleftarrows P_2 \qquad [R23]$$

This reaction is exergonic being $\Delta_r G^o_{298K}$ R23 = −15 kJ mol^{-1}. The addition of another water molecule leads to the loss of oxalic acid and the formation of P_3 (see Fig. 5a). This reaction is strongly exergonic and $\Delta_r G^o_{298K}$ R24 = −49 kJ mol^{-1}:

$$P_2 + H_2O \rightleftarrows P_3 + H_2C_2O_4(sol) \qquad [R24]$$

The hydrolysis degradation proceeds with the loss of a second molecule of oxalic acid and the formation of boric acid R25:

$$P_3 + H_2O \rightleftarrows H_3BO_3(sol) + H_2C_2O_4(sol) \qquad [R25]$$

The last step is exergonic given that $\Delta_r G^o_{298K}$ R25 = −27 kJ^{-1} mol. Although R23, R24 and R25 are widely exergonic, the large positive energy difference observed in R22 hinders this hydrolysis path.

Discussion

The comparison between the hydrolysis mechanisms of $LiBF_4$, LiODBF and LiBOB (see Fig. 6) allows to identify two possible reaction paths:

1. LiF(s) precipitation and HF release;
2. LiOH(s) precipitation.

The first type mechanism is thermodynamically viable at room temperature; in fact, the hydrolytic path for fluorine-containing salts is exergonic or weakly endergonic. $LiBF_4$ can easily hydrolyze, whereas LiODBF shows a small Gibbs energy difference between reagents and products ($\Delta_r G^o_{298K}$ = 19 kJ mol^{-1}). This barrier is only

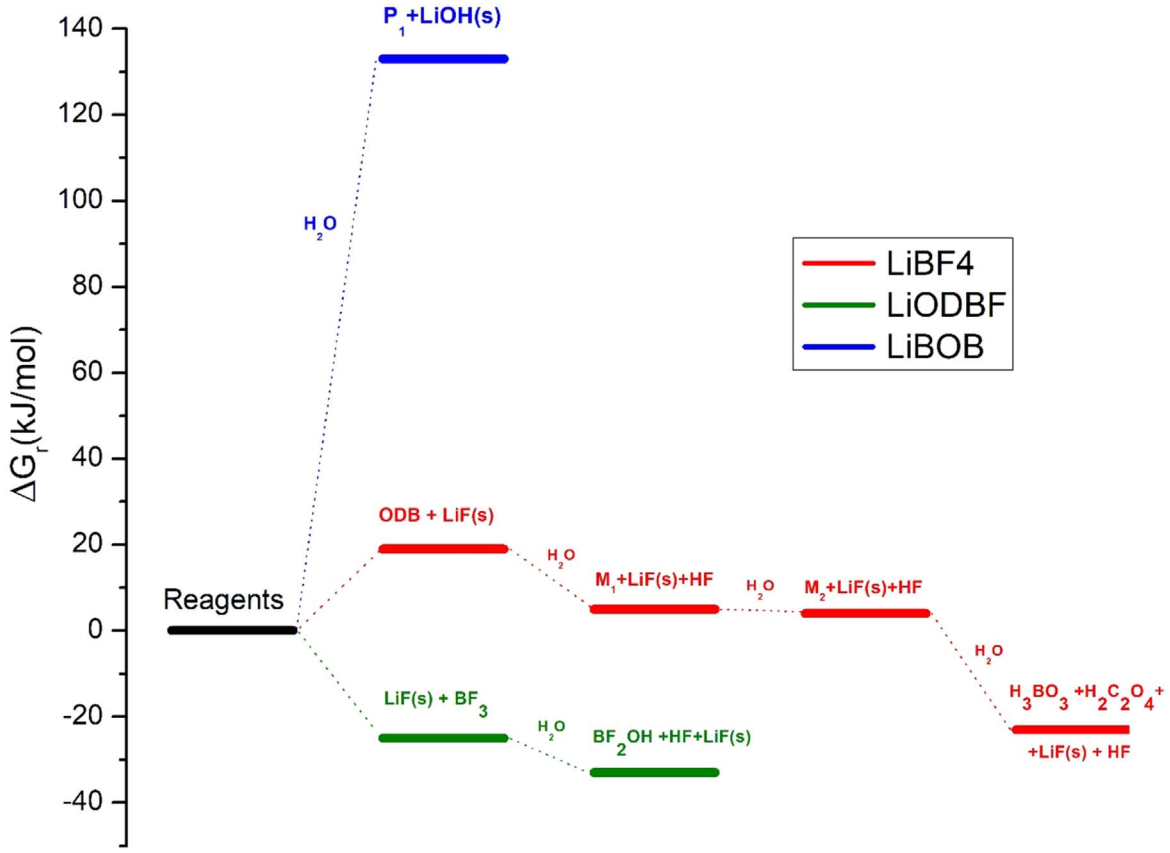

Figure 6. Comparative thermodynamic landscape of the hydrolysis of borate-base lithium salts. Numerical values close to the energy levels are the corresponding Gibbs energy differences compared to reagents.

slightly altered by the temperature, being $\Delta_r G^o_{248K} = 15$ kJ mol^{-1}, $\Delta_r G^o_{298K} = 19$ kJ mol^{-1} and $\Delta_r G^o_{348K} = 23$ kJ mol^{-1}. The second path, i.e. the LiOH(s) precipitation, is thermodynamically irrelevant at room temperature for all salts, due to the extremely high positive Gibbs energy variations. It is of interest to underline that apparently all the coordination of lithium ions in the solution to form chelating adducts with intermediate species are unlikely to occur being endergonic the corresponding Gibbs energy of reactions at 298 K (see Table SVII in the SI).

Overall, the precipitation of lithium fluoride and the release of hydrofluoric acid is the driving force of the hydrolysis of these fluorinated salts, leading to BF_2OH as the main degradation byproduct. In fact, the formation of BF_2OH in the pathway of hydrolysis of $LiBF_4$ is the possible thermodynamic endpoint of the fluoroborate hydrolysis. LiBOB does not contain fluorine atoms: thus the direct reaction with water exhibits only an insurmountable thermodynamic energy difference at room temperature to precipitate LiOH(s). From a kinetic point of view the energy barrier is even higher in consideration to the inevitable additional activation energy to initiate the reaction. This means that LiBOB is stable in presence of traces of water and the degradation of this salt likely occurs through more complex mechanisms, probably driven by electrochemical reduction/oxidation processes.

As a final point, we must consider the possible driving force to form solid lithium borate or lithium oxalate. In fact, the formation of boric acid, although in traces, can feed another reaction, R26, between H_3BO_3 and $LiBF_4$, to form $LiBO_2$(s):

$$H_3BO_3(sol) + LiBF_4(sol) \rightleftarrows LiBO_2(s) + BF_3 + HF + H_2O \quad \text{[R26]}$$

Similarly, the formation of solid lithium oxalate must be considered in view of the reaction between $H_2C_2O_4$(sol) and LiODBF, R27:

$$H_2C_2O_4(sol) + LiODBF \rightleftarrows Li_2C_2O_4(s) + 2ODBF + 2HF \quad \text{[R27]}$$

However, both R26 and R27 are endergonic, being $\Delta_r G^o_{298K}$ R26 $= 46$ kJ mol^{-1} and $\Delta_r G^o_{298K}$ R27 $= 291$ kJ mol^{-1}, respectively, and it is, therefore, unlikely that $LiBO_2$ and $Li_2C_2O_4$ nucleate as final byproducts of borate-based salt hydrolysis.

Conclusions

In this work we studied the thermodynamics of hydrolysis of $LiBF_4$, LiODBF and LiBOB, as these salts are commonly used in lithium-ion batteries. We performed density functional theory calculations to compute the thermodynamic stability of reagents, reaction intermediates and products. We exploited thermochemical cycles to describe the realistic thermodynamic landscape of hydrolysis mechanisms, coupling literature assessed values for solid compounds (LiOH(s), LiF(s), H_3BO_3(s) and $H_2C_2O_4$(s)) with the quantities obtained by DFT calculations. We investigated the direct reaction of salts with water, observing two general reaction paths. The first is driven by the precipitation of lithium fluoride and the release of hydrofluoric acid, while the second one by the formation of lithium hydroxide. $LiBF_4$ and LiODBF likely react with water following both pathways; however, the degradation through the LiF (s)/HF channel is strongly favored. On the other hand, the F-free LiBOB salt is much more stable and apparently does not react with water following a simple chemical path. The degradation of LiBOB in LIBs electrolytes is probably driven by other more complex mechanisms, involving oxidation/reduction processes and will be the object of a future focused work.

Acknowledgments

The authors would like to acknowledge the financial support from the European Union Horizon 2020 research and innovation program within the Si-DRIVE project; grant agreement No. 814464. This manuscript is dedicated to Prof. Guido Gigli for his mentoring, tutoring and extraordinary teachings in the field of physical chemistry.

ORCID

Sergio Brutti https://orcid.org/0000-0001-8853-9710

References

1. S. Passerini and B. Scrosati, "Lithium and lithium-ion batteries: Challenges and prospects." *Electrochem. Soc. Interface*, **25**, 85 (2016).
2. B. Scrosati and J. Garche, "Lithium batteries: Status, prospects and future." *J. Power Sources*, **195**, 2419 (2010).
3. M. Ue and S. Mori, "Mobility and Ionic Association of Lithium Salts in a Propylene Carbonate-Ethyl Methyl Carbonate Mixed Solvent." *J. Electrochem. Soc.*, **142**, 2577 (1995).
4. E. M. Wigayati, T. Lestariningsih, A. Subhan, C. R. Ratri, and I. Purawiardi, "Synthesis and characterization of LiBOB as electrolyte for lithium-ion battery." *Ionics*, **22**, 43 (2016).
5. M. Xu, L. Zhou, L. Hao, L. Xing, W. Li, and B. L. Lucht, "Investigation and application of lithium difluoro(oxalate)borate (LiDFOB) as additive to improve the thermal stability of electrolyte for lithium-ion batteries." *J. Power Sources*, **196**, 6794 (2011).
6. R. Younesi, G. M. Veith, P. Johansson, K. Edström, and T. Vegge, "Lithium salts for advanced lithium batteries: Li-metal, Li-O2, and Li-S." *Energy Environ. Sci.*, **8**, 1905 (2015).
7. S. Hwang, D. Kim, J. H. Shin, K. H. Ahn, C. Lee, and H. Lee, "Ionic conduction and solution structure in lipf6 and $LiBF_4$ propylene carbonate electrolytes." *J. Phys. Chem. C*, **122**, 19438 (2018).
8. S. S. Zhang, K. Xu, and T. R. Jow, "Study of $LiBF_4$ as an electrolyte salt for a Li-Ion battery." *J. Electrochem. Soc.*, **149**, A586 (2002).
9. S. S. Zhang, K. Xu, and T. R. Jow, "Low-temperature performance of Li-ion cells with a $LiBF_4$-based electrolyte." *J. Solid State Electrochem.*, **7**, 147 (2003).
10. H. Lee, M. Yanilmaz, O. Toprakci, K. Fu, and X. Zhang, "A review of recent developments in membrane separators for rechargeable lithium-ion batteries." *Energy Environ. Sci.*, **7**, 3857 (2014).
11. C. Yang, H. Tong, C. Luo, S. Yuan, G. Chen, and Y. Yang, "Boehmite particle coating modified microporous polyethylene membrane: A promising separator for lithium ion batteries." *J. Power Sources*, **348**, 80 (2017).
12. M. T. F. Rodrigues, C. Liao, K. Kalaga, I. A. Shkrob, and D. P. Abraham, "Dehydration rather than HF capture explains performance improvements of Li-Ion cells by ceramic nanoparticles." *ACS Appl. Energy Mater.*, **2**, 5380 (2019).
13. M. Agostini, A. Matic, S. Panero, F. Croce, R. Gunella, P. Reale, and S. Brutti, "A mixed mechanochemical-ceramic solid-state synthesis as simple and cost effective route to high-performance $LiNi_{0.5}Mn_{1.5}O_4$ spinels." *Electrochim. Acta*, **235**, 262 (2017).
14. P. Verma, P. Maire, and P. Novák, "A review of the features and analyses of the solid electrolyte interphase in Li-ion batteries." *Electrochim. Acta*, **55**, 6332 (2010).
15. F. Gao, X. Tian, J. Lin, J. Dong, X. Lin, and J. Li, "In situ raman, FTIR, and XRD spectroscopic studies in fuel cells and rechargeable batteries." *Nano Res.* (2022).
16. S. Narayanan, J. S. Gibson, J. Aspinall, R. S. Weatherup, and M. Pasta, "In situ and operando characterisation of Li metal—solid electrolyte interfaces." *Curr. Opin. Solid State Mater. Sci.*, **26**, 100978 (2022).
17. S. Shi, P. Lu, Z. Liu, Y. Qi, L. G. Hector, H. Li, and S. J. Harris, "Direct calculation of Li-ion transport in the solid electrolyte interphase." *JACS*, **134**, 15476 (2012).
18. A. Wang, S. Kadam, H. Li, S. Shi, and Y. Qi, "Review on modeling of the anode solid electrolyte interphase (SEI) for lithium-ion batteries." *NPJ Comput. Mater.*, **4**, 15 (2018).
19. S. Bertolini and P. B. Balbuena, "Buildup of the solid electrolyte interphase on lithium-metal anodes: reactive molecular dynamics study." *J. Phys. Chem. C*, **122**, 10783 (2018).
20. A. A. Franco, A. Rucci, D. Brandell, C. Frayet, M. Gaberscek, P. Jankowski, and P. Johansson, "Boosting Rechargeable Batteries R&D by Multiscale Modeling: Myth or Reality? " *Chem. Rev.*, **119**, 4569 (2019).
21. K. L. Browning, L. Baggetto, R. R. Unocic, N. J. Dudney, and G. M. Veith, "Gas evolution from cathode materials: A pathway to solvent decomposition concomitant to SEI formation." *J. Power Sources*, **239**, 341 (2013).
22. C. G. Barlow, "Reaction of Water with Hexafluorophosphates and with Li Bis (perfluoroethylsulfonyl)imide Salt." *Electrochem. Solid-State Lett.*, **2**, 362 (1999).
23. M. Amereller, M. Multerer, C. Schreiner, J. Lodermeyer, A. Scmid, J. Barthel, and H. J. Gores, "Investigation of the hydrolysis of lithium bis[1,2-oxalato(2-)−0,0] borate (LiBOB) in water and acetonitrile by conductivity and NMR measurements in comparison to some other borates." *J. Chem. Eng. Data*, **54**, 468 (2009).
24. M. E. Jacox, K. K. Irikura, and W. E. Thompson, "The reaction of BF_3 with H2O: Infrared spectrum of BF_2OH trapped in solid neon." *J. Chem. Phys.*, **113**, 5705 (2000).
25. N. P. W. Pieczonka, L. Yang, M. P. Balogh, B. R. Powell, K. Chemelewski, A. Manthiram, S. A. Krachkovsky, G. R. Goward, M. Liu, and J. Kim, "Impact of lithium bis(oxalate)borate electrolyte additive on the performance of high-voltage spinel/graphite Li-ion batteries." *J. Phys. Chem. C*, **117**, 22603 (2013).
26. K. Xu, S. S. Zhang, U. Lee, J. L. Allen, and T. R. Jow, "LiBOB: Is it an alternative salt for lithium ion chemistry? in." *J. Power Sources*, **146**, 79 (2005).
27. J. Yu, N. Gao, J. Peng, N. Ma, X. Liu, C. Shen, K. Xie, and Z. Fang, "Concentrated LiODFB electrolyte for lithium metal batteries." *Frontiers in Chemistry*, **7**, 494 (2019).
28. S. Di Muzio, A. Paolone, and S. Brutti, "Thermodynamics of the hydrolysis of lithium salts: pathways to the precipitation of inorganic SEI components in Li-Ion batteries." *J. Electrochem. Soc.*, **168**, 100514 (2021).
29. Y. Shao et al., "Advances in methods and algorithms in a modern quantum chemistry program package." *Phys. Chem. Chem. Phys.*, **8**, 3172 (2006).
30. N. Mardirossian and M. Head-Gordon, "ω B97M-V: A combinatorially optimized, range-separated hybrid, meta-GGA density functional with VV10 nonlocal correlation." *J. Chem. Phys.*, **144**, 214110 (2016).
31. A. D. McLean and G. S. Chandler, "Contracted Gaussian basis sets for molecular calculations. I. Second row atoms, Z = 11-18." *J. Chem. Phys.*, **72**, 5639 (1980).
32. M. Cossi, N. Rega, G. Scalmani, and V. Barone, "Energies, Structures, and Electronic Properties of Molecules in Solution with the C-PCM Solvation Model." *J. Comput. Chem.*, **24**, 669 (2003).
33. T. Yanai, D. P. Tew, and N. C. Handy, "A new hybrid exchange-correlation functional using the Coulomb-attenuating method (CAM-B3LYP)." *Chem. Phys. Lett.*, **393**, 51 (2004).
34. M. W. Chase Jr, "NIST-janaf thermochemical tables." *J. Phys. Chem. Ref. Data, Monograph* (American Chemical Society, New York, NY) 1510 (1998), American Institute of Physics for the National Institute of Standards and Technology.
35. R. F. Porter, D. R. Bidinosti, and K. F. Watterson, "Mass spectrometric study of the reactions of BF_3(g) with BCl3(g), B(OH)3(g), and B2O3(1)." *J. Chem. Phys.*, **36**, 2104 (1962).
36. D. L. Hildenbrand, L. P. Theard, and A. M. Saul, "Transpiration and mass spectrometric studies of equilibria involving BOF(g) and (BOF)3(g)." *J. Chem. Phys.*, **39**, 1973 (1963).
37. J. O. Jensen, "Vibrational frequencies and structural determination of trifluoroboroxine." *J. Mol. Struct. THEOCHEM*, **676**, 193 (2004).
38. M. E. Jacox, K. K. Irikura, and W. E. Thompson, "The reaction of BF_3 with H2O: Infrared spectrum of f BF_2OH trapped in solid neon." *J. Chem. Phys.*, **113**, 5705 (2000).